Korean J. Chem. Eng., 39(11), 3048-3054 (2022)
DOI: 10.1007/s11814-022-1207-z

pISSN: 0256-1115
eISSN: 1975-7220

Enhanced adsorption of lead ions by enzymatically synthesized poly(*m*-phenylenediamine)-graphene oxide composites

Bharat Bhargawa*,‡, Yue Xu,‡, Ik-Keun Yoo*, Sung Gu Kang*, and Keungarp Ryu*,†**

*Department of Chemical Engineering, College of Engineering, University of Ulsan, Ulsan 44610, Korea
**School of Chemistry and Chemical Engineering, Shanghai University of Engineering Science, Shanghai, China
(*Received 4 February 2022 • Revised 9 June 2022 • Accepted 12 June 2022*)

Abstract−Adsorption is considered efficient for removing metal ions dissolved in aquatic environments. For the successful performance of adsorption processes, the development of adsorbents possessing high adsorption capacity is essential. Herein, we report the enzymatic synthesis of composites consisting of *m*-phenylenediamine polymer (pmPDA) and graphene oxide (GO) by laccase and the adsorption properties of these composites for Pb^{2+}, a representative toxic metal ion. Especially, the composite synthesized with initial 1 : 1 mass ratio of *m*-phenylenediamine monomer and GO was found to have the largest adsorption capacity for Pb^{2+}. The Langmuir isotherm for the adsorption of Pb^{2+} by GO, pmPDA, and this composite, respectively, revealed that the maximum adsorption capacity, q_{max}, of this composite was the highest (2,164 μmol/g) being almost four times higher than that for pmPDA (564.7 μmol/g). The q_{max} for GO was 984.3 μmol/g being about two times higher than for pmPDA but less than a half of q_{max} for this composite. The composite was estimated to contain 56.1 wt% of pmPDA as examined by thermogravimetric analysis. This study demonstrates that the combination of the high surface area of GO and the functionality of pmPDA can significantly enhance the adsorption capacity for Pb^{2+}.

Keywords: Adsorption, Graphene Oxide, Lead Ions, Laccase, *m*-Phenylenediamine Polymer

INTRODUCTION

Modern chemical industries are highly dependent on metals and trace elements as catalysts; thus, they are known to create waste effluents containing numerous pollutants, including organic, inorganic, and organometallic chemical waste [1]. Particularly, the presence of heavy metal ions in water resources becomes a serious concern as heavy metals are hard to process, thus resulting in bioaccumulation and further affecting the biological and ecological food chain. Heavy metals like Cr, Cd, As, Ni, Hg and Pb are well-known to cause several deformities to human health and are also potent carcinogens [2]. To date, several treatment methods have been tried and tested for the efficient removal of lethal pollutants from the wastewater effluents including membrane filtration, chemical precipitation, ion exchange, coagulation-flocculation, adsorption, and electrochemical treatments [3-7]. Most of these technologies, however, suffer from major limitations such as extreme running cost, insignificant efficiency at usual discharge stages, and production of residual toxic sludge along with secondary wastes [8,9]. Among these techniques, the adsorption method is considered simple, cost-effective, and flexible to adapt to various operational environments [4]. Hence, the adsorption methods of heavy metals have been actively investigated using several adsorbent materials, such as activated carbons, polymers, and bio-sorbents [10-12].

Recently, polymers containing aromatic amines and diamines have emerged as effective carriers for the adsorptive removal of contaminants, as these polymers hold numerous amine functional groups and exhibit great thermal stability [13]. Specifically, phenylenediamine polymers were found to be one of the most successful adsorbents against various heavy metal ions such as Pb^{2+}, Ag^{+}, and Cr^{6+} [10,14,15]. Meanwhile, carbon-based materials, such as carbon nanotubes, graphene and their derivatives, are popular choices for adsorptive research due to the advantages they hold including high electrical conductivities, exceptional mechanical strength, decent chemical stability, and large surface area [16]. Among these materials, graphene oxide (GO) is the most favorable carbon nanomaterial that has numerous oxygen-containing functional groups, for example, carbonyl, hydroxyl, carboxyl groups [17]. Thus, GO has been extensively utilized to make stable multifunctional composites for various applications in the areas of electronics, supercapacitors, chemical sensors, biosensors etc [18-21]. Interestingly, polymers' high thermal stability, metal ions affinity, and ease of synthesizing flexibility go perfectly well with the high surface areas and oxygen functional groups of GO.

Generally, polymers and their carbon nanomaterial-based composites have been synthesized via harsh chemical oxidation reactions. These chemical procedures are mostly driven by strong oxidants in extremely acidic conditions, therefore, not considered eco-friendly [10]. Unlike the chemical polymerization process, the enzymatic approach performs reactions under mild conditions without using harmful oxidants, extreme temperature, or generating secondary lethal by-products. Furthermore, the nano-scale structures of carbon nanotubes and graphene were found to remain intact under

†To whom correspondence should be addressed.
E-mail: kgryu@ulsan.ac.kr
‡Co-first authors

enzymatic reaction conditions [22]. Thus, enzymatic reaction systems have been considered a replacement for the traditional chemical methods to create eco-friendly synthetic processes. Specifically, peroxidases and oxidases which are capable to oxidize various substituted phenols and aromatic amines have attracted much attention to replace the corresponding chemical processes [23-25]. As we reported earlier, laccase and horseradish peroxidase have great potential to catalyze the synthesis of multi-walled carbon nanotubes-polypyrrole (MWCNTs-PPy) [22,26] and graphene oxide-polypyrrole (GO-PPy) composites via simple enzymatic catalysis [27].

In our previous report, we successfully synthesized *m*-phenylenediamine polymer (pmPDA) by utilizing laccase isolated from *Trametes versicolor* as a catalyst in a moderate aqueous condition [28]. In this paper, we report the synthesis of various GO-pmPDA composites by laccase and their adsorptive properties for highly toxic metal ion, Pb^{2+} in water. We also demonstrate that for a composite possessing the advantages of pmPDA for abundant functionality and GO for high surface area, the adsorptive capacity for Pb^{2+} can be enhanced markedly.

EXPERIMENTAL

1. Materials

Laccase (Sigma 53739) produced from *Trametes versicolor*, which was found to be a single enzyme (molecular weight 66 kDa) [26], *m*-phenylenediamine, and $Pb(NO_3)_2$ were purchased from Sigma-Aldrich and used without further purification. GO was synthesized starting from expanded graphite using the modified Hummers method [29].

2. The Enzymatic Synthesis of GO-pmPDA Composites

The laccase-catalyzed enzymatic synthesis of pmPDA and GO-pmPDA composites were performed in aqueous solutions as previously described [28,30]. In detail, a 30 mL buffer (10 mM citrate phosphate buffer, pH 3) was aerated before the reaction. Then 200 mg GO and 10 mg of laccase were added into the buffer. Next, different amounts of *m*-phenylenediamine monomer (50, 100, 200, 300, and 400 mg, respectively) were added to the buffer solution to initiate the simultaneous polymerization of the *m*-phenylenediamine monomer and the synthesis of the composites. To synthesize pmPDA alone, 200 mg *m*-phenylenediamine and 10 mg laccase were mixed in 30 mL of the same buffer in the absence of GO. After the agitation of the reaction solutions for 24 h at 25 °C, the reaction solutions were filtered on a nylon membrane (0.2 μm). The filtered out precipitant was washed with distilled water, then with methanol. The washed pmPDA and GO-pmPDA composites were dried under vacuum. The various GO-pmPDA composites produced were named GO-P50, GO-P100, GO-P200, GO-P300, and GO-P400 to indicate the different initial amounts of *m*-phenylenediamine used (50, 100, 200, 300, and 400 mg, respectively). The precise production yields of the final dried composites were difficult to measure due to the adhesion of the composites on the filtering equipment and the filtering membrane. However, the approximate yields of the dried pmPDA and GO-pmPDA composites were in the range of 50-90%.

The surface morphological properties of GO-pmPDA composites were investigated by scanning electron microscopy (SEM) (Supra 40, Carl Zeiss, Swiss). The polymer content and thermal stability of composites were analyzed using thermogravimetric analysis (TGA) on TGA Q50 from 25 °C to 800 °C under N_2 at a heating rate of 10 °C/min as previously described [28].

3. Adsorption Experiment of Pb^{2+}

Batch-type adsorption experiments were performed as described below. All the experiments were carried out by taking 5 mg of GO, pmPDA, or a GO-pmPDA composite as an adsorbent in centrifuge tubes containing 10 mL adsorption solution. The adsorption solutions were sonicated for 30 min to avoid aggregation of the adsorbent particles before adding Pb^{2+} ions. In our previous report, we observed the importance of pH for the adsorption of Pb^{2+} ions by pmPDA; the adsorption capacity was maximum in distilled water and decreased as the solution became more acidic [30]. Therefore, the adsorption process was performed in distilled water with gentle shaking for 12 h at 25 °C. Later, the adsorption solutions were centrifuged to separate the adsorbent. The concentration of dissolved Pb^{2+} ions in the supernatant was then estimated using an atomic absorption spectrophotometer (Shimadzu AA-7000). Control experiments were also performed in the absence of absorbents but with each concentration of dissolved Pb^{2+} ions. And then, full recovery of the initial amounts of Pb^{2+} ions was affirmed for the control experiments. The existence of adsorbed Pb^{2+} ions on the GO-pmPDA composites after the adsorption experiments was verified by scanning electron microscopy-energy dispersive spectrum (SEM-EDS) analysis (JSM-7600F field emission scanning electron microscope, JEOL, Japan).

The adsorbed amount of Pb^{2+} ions was estimated from the difference in the dissolved metal ion concentration between the initial and final adsorption solutions as Eq. (1):

$$q=(C_i-C)\,V/M \tag{1}$$

where q (μmol/g) is the adsorbed amount of metal ions, M (g) is the mass of the used adsorbent, V (L) the volume of the metal ion solution and C_i and C are the concentrations (μmol/L) of the metal ions in the initial solution before adding the adsorbent and in the final solution after the adsorption, respectively.

4. The Estimation of pmPDA Contents in the GO-pmPDA Composites Using TGA

The content of pmPDA in the GO-pmPDA composites was estimated by using the two-temperature method proposed by Nabinejad et al. [31]. The detailed steps for the estimation are described below.

The total mass of a GO-pmPDA composite is the sum of the individual masses of pmPDA and GO contained in the composite as in Eq. (2). Thereby, the mass percentage of pmPDA (P_p) can be expressed by Eq. (3).

$$m_c=m_p+m_{go} \tag{2}$$

$$P_p=100\ m_p/m_c \tag{3}$$

In the above equations, m_c is the initial mass of the GO-pmPDA composite and m_p and m_{go} are the initial masses of pmPDA and GO contained in the composite, respectively, before thermal degradation.

At a high temperature T_d,

$$m_{dc}=P_{dp}\, m_p/100+P_{dgo}\, m_{go}/100 \quad (4)$$

where m_{dc} is the decreased mass of the composite and P_{dp} and P_{dgo} are the percentage mass decreases of pmPDA and GO at T_d, respectively.

At another higher temperature T_r,

$$m_{rc}=P_{rp}\, m_p/100+P_{rgo}\, m_{go}/100 \quad (5)$$

where m_{rc} is the mass residue of the composite, and P_{rp} and P_{rgo} are the mass percentage residues of pmPDA and GO at T_r, respectively.

From Eq. (4),

$$m_{go}=100\, m_{dc}/P_{dgo}-P_{dp}\, m_p/P_{dgo} \quad (6)$$

Substituting Eq. (6) into Eq. (5) for m_{go},

$$m_p=\alpha m_{dc}+\beta m_{rc} \quad (7)$$

where

$$\alpha=100\, P_{rgo}/(P_{rgo}\, P_{dp}-P_{rp}\, P_{dgo}) \quad (8)$$

and

$$\beta=100\, P_{dgo}/(P_{rp}\, P_{dgo}-P_{rgo}\, P_{dp}) \quad (9)$$

Finally,

$$P_p=100\, m_p/m_c=100\, (\alpha\, m_{dc}+\beta\, m_{rc})/m_c=\alpha\, P_{dc}+\beta\, P_{rc} \quad (10)$$

where, P_{dc} and P_{rc} are the percentage mass decrease at T_d and the percentage mass residue at T_r of the composite, respectively. Note that α and β values in Eq. (10) can be calculated from the thermal degradation properties of GO and pmPDA separately according to Eqs. (8) and (9).

RESULTS AND DISCUSSION

1. The Morphological Studies

We investigated the surface morphology of GO, pmPDA, and GO-pmPDA composites by using scanning electron microscopy (SEM) and the results are shown in Fig. 1. At low magnification (x1,000) SEM image of GO (Fig. 1(a)), thin GO flakes that are well separated individually can be observed. At higher magnification (x10,000) SEM image of GO, GO shows a thin smooth lamellar structure with a few folds. Whereas, Fig. 1(c) shows that pmPDA synthesized by laccase has the shape of agglomerated globular particles with diameters less than 1 μm as also previously observed [28]. Fig. 1(d) to Fig. 1(h) for the GO-pmPDA composites indicate that the surface of GO sheets is covered with pmPDA particles at different proportions. The contacting interface between GO and pmPDA seems very weak and can be distinguished easily. Interestingly, as the pmPDA content increased from GO-P50 to GO-P400, more pmPDA particles took the available surface of GO to a larger extent. Notably, pmPDA globules on GO surfaces for GO-

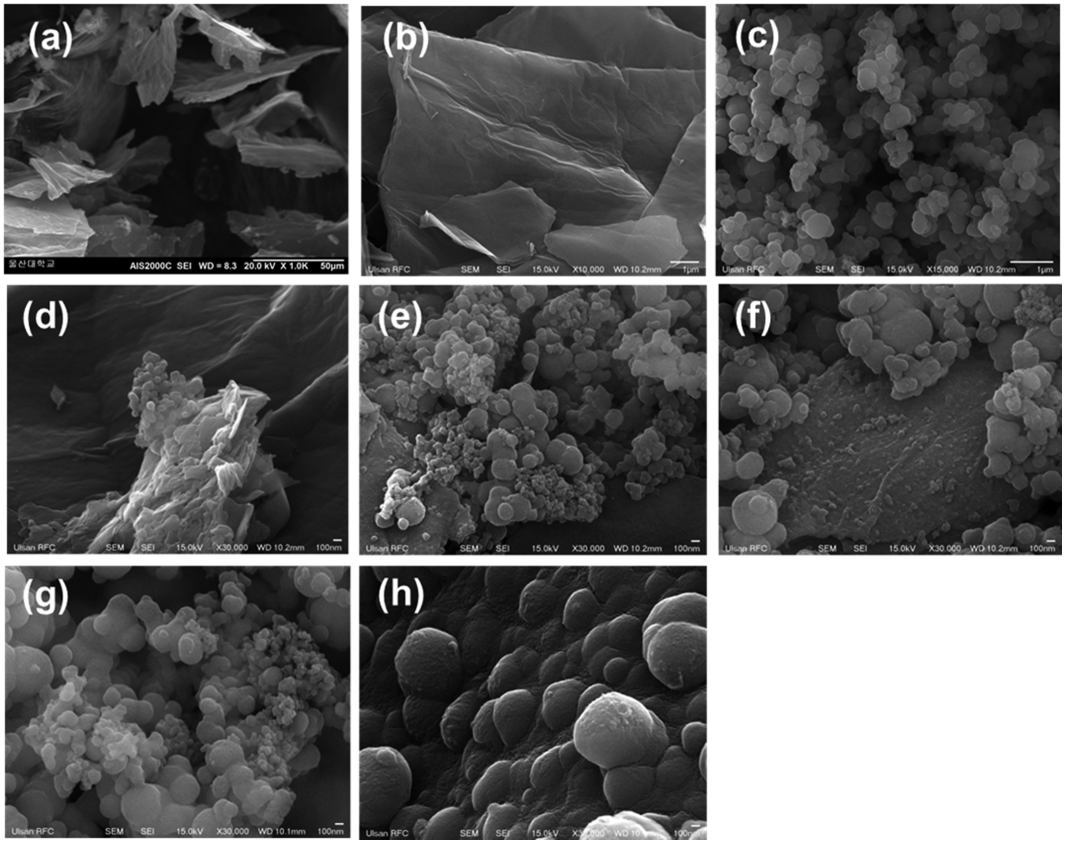

Fig. 1. SEM images of GO (a), (b), pmPDA (c), and GO-pmPDA composites; GO-P50, GO-P100, GO-P200, GO-P300, and GO-P400 (d)-(h). Magnifications are 1 k (a) and 10 k (b) for GO, 15 k for pmPDA (c), and 30 k for GO-pmPDA composites (d)-(h). Scale bars are 50 μm for GO (a), 1 μm for GO (b) and pmPDA (c), and 100 nm for GO-pmPDA composites (d)-(h).

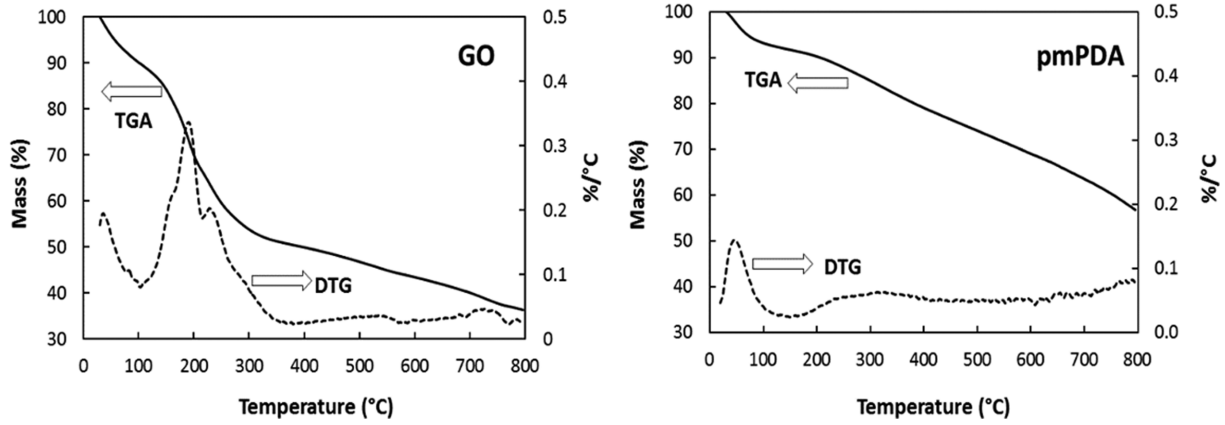

Fig. 2. TGA and DTG (Difference Thermogravimetry) plots of GO (left) and pmPDA (right).

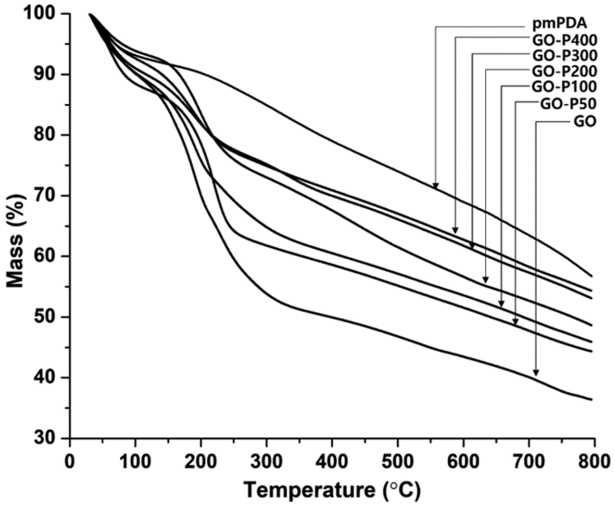

Fig. 3. TGA thermograms of GO, pmPDA, and GO-pmPDA composites.

P400 composite (Fig. 1(h)) had the largest sizes among the GO-pmPDA composites possibly due to the initiation and growth of the polymer on the GO surfaces in the presence of abundant mPDA monomers. However, Fig. 1(c) shows that pmPDA particles synthesized in the absence of GO had smaller and rather uniform sizes, presumably because of the countless simultaneous initiation of the polymerization catalyzed by laccase dissolved in the solution.

2. Thermogravimetric Analysis and the Estimation of the Contents of GO-pmPDA Composites

The thermal stability of various composites was analyzed by TGA and compared with a pure form of GO and pmPDA as shown in Fig. 2 and Fig. 3. The thermal stability of GO is much weaker than the pmPDA. Fig. 3 shows TGA curves for the GO-pmPDA composites also from 0 to 800 °C. At high temperatures, pmPDA has the highest mass residue, whereas GO has the lowest. As a result, the addition of a greater amount of pmPDA to the composites tended to increase the mass residue of the GO-pmPDA composite, which moved closer to the mass residue of pmPDA.

Table 1. Parameter values of TGA data for GO and pmPDA

Sample	GO	pmPDA
Percent decrease at T_d (400 °C)	P_{dgo}=50.07	P_{dp}=20.99
Percentage residue at T_r (650 °C)	P_{rgo}=41.90	P_{rp}=66.43
α=−1.7125		
β=2.0465		

For the estimation of the polymer content in the GO-pmPDA composites, as proposed by Nabinejad et al. [31], T_d was determined as the temperature (400 °C) below which most thermal degradation occurred for GO and pmPDA, as shown in the DTG diagrams of GO and pmPDA (Fig. 3). T_r was selected as the temperature (650 °C) where most composites exhibited the thermal degradation of the similar constant slopes (Fig. 3).

The measured parameters of thermal degradation and the calculated values of α and β from Eqs. (8) and (9) for GO and pmPDA are listed in Table 1. The estimated content of pmPDA in the GO-pmPDA composites calculated from Eq. (10) is presented in Table 2 with the values of T_d and T_r being 400 °C and 650 °C, respectively. GO-P50 exhibited the lowest mass percentage of pmPDA of 30.8 wt%, whereas GO-P400 was estimated to have the highest mass percentage of pmPDA of 72.9 wt%. GO-P200 showed a moderate mass percentage of pmPDA of 56.1 wt%.

3. Preliminary Adsorption Studies

We performed the initial experiment to assess and compare the adsorption capability of GO, pmPDA, and various GO-pmPDA

Table 2. The pmPDA contents in the various composites estimated from TGA

Sample	GO-P50	GO-P100	GO-P200	GO-P300	GO-P400
Percent decrease (P_{dc}) at T_d (400 °C)	41.4	39.5	32.4	30.0	29.9
Percentage residue (P_{rc}) at T_r (650 °C)	49.7	51.7	54.6	59.4	60.6
wt% of pmPDA	30.8	38.2	56.1	70.2	72.9

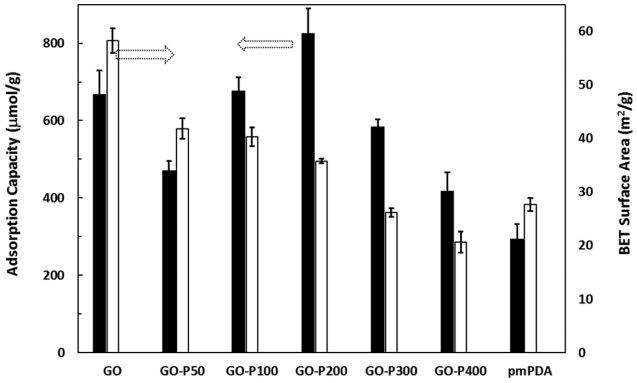

Fig. 4. The Pb^{2+} adsorption capacity (filled bar) and BET surface area (blank bar) of GO, pmPDA, and GO-pmPDA composites. Data are the averages of triplicate measurements. Adsorption mixtures containing 5 mg of each adsorbent and 150 mg/L of $Pb(NO_3)_2$ in 10 mL distilled water were shaken for 12 h at 25 °C.

composites for the adsorption of Pb^{2+} ions with the initial $Pb(NO_3)_2$ concentration of 150 mg/L and the results are presented in Fig. 4. The pmPDA was found to have the lowest adsorption capacity of 295 μmol/g, whereas the GO-P200 composite exhibited the highest adsorption capability of 825 μmol/g. The adsorption capacity of pure GO was 669 μmol/g, twice that of pmPDA.

To gain more information regarding surface structural properties associated with the adsorption capability of the adsorbents, GO, pmPDA, GO-pmPDA composites were analyzed for the Brunauer-Emmett-Teller (BET) surface areas. As also shown in Fig. 4, The BET surface area of the pmPDA was 27.62 m^2/g compared to the largest surface area of 58.24 m^2/g for GO. As the content of pmPDA increased in the composites, the surface area continued to decrease and dropped significantly for GO-P300 (26.15 m^2/g) and GO-P400 (20.59 m^2/g), which were estimated to contain more than 70 wt% of pmPDA. GO-P200, which showed the highest adsorption capacity and estimated to possess 56.1 wt% of pmPDA, had its surface area of 35.75 m^2/g. The lower surface area of GO-P400 than pmPDA alone may be attributed to the partly decreased available surface area of the large polymer globules attached on the surface of GO (Fig. 1(h)).

The surface area of absorbents is generally considered an important factor to determine the adsorption capability of the materials. In Fig. 4, however, it is obvious that the adsorption capacities of the adsorbents are not in direct proportion to their surface areas. The GO and pmPDA contain oxygen and amine groups, respectively, which can bind positive metal ions through electrostatic attractive forces. Therefore, it can be presumed that the optimum combination of the high surface area of GO and the functionalities of GO and pmPDA became the important factor to enable the highest adsorption capability of GO-P200.

The inclusion of Pb^{2+} ions in the GO-pmPDA composites after the adsorption experiments was directly verified by SEM-EDS analysis of GO-P200 composites as shown in Fig. 5. The SEM-EDS analysis of the GO-P200 composites before the adsorption shows no peaks for Pb^{2+} ions. After the adsorption, however, SEM-EDS for the composites clearly shows peaks for Pb^{2+} ions near 2-3 keV. These results prove that Pb^{2+} ions are adsorbed on the GO-P200 composites even after the removal of weakly bound Pb^{2+} ions by washing the composites with distilled water following the filtration of the adsorption solution.

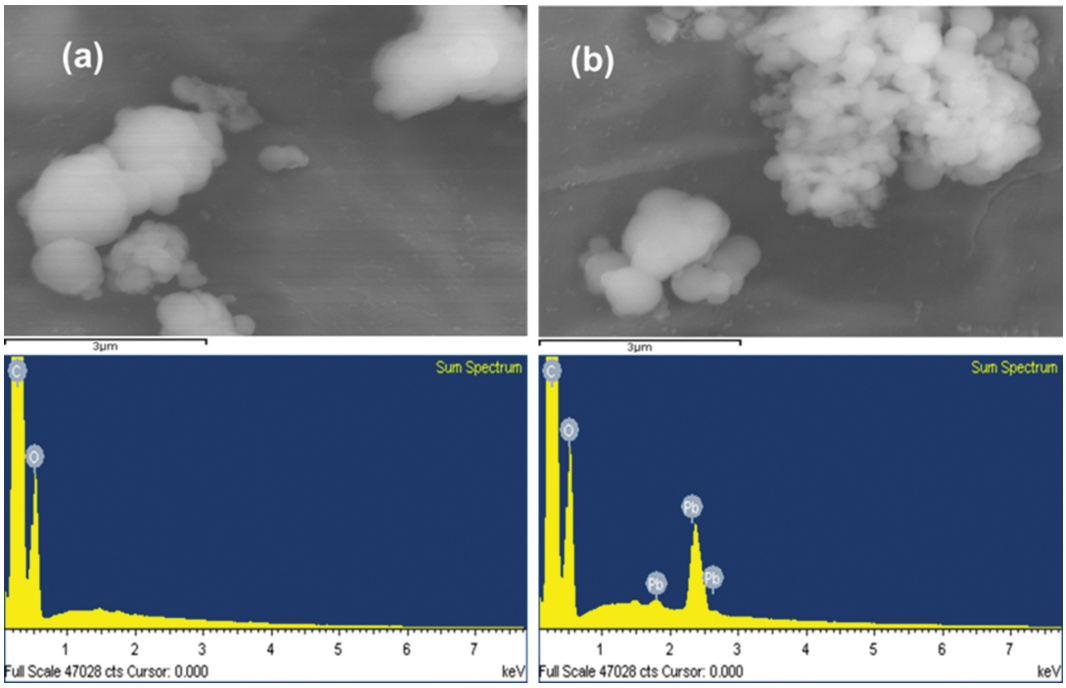

Fig. 5. SEM-EDS analysis (magnification of 15 k) of the GO-P200 composites before (a) and after (b) the Pb^{2+} adsorption. After the adsorption experiments with 150 mg/L of $Pb(NO_3)_2$, the GO-P200 composites were filtered on a nylon membrane (0.2 μm) then washed with distilled water. The composites were then dried under vacuum for the SEM-EDS analysis.

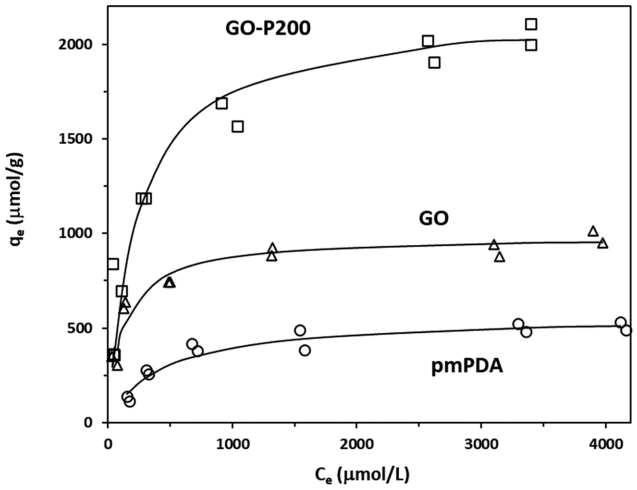

Fig. 6. Adsorption isotherms for Pb^{2+} on GO and the enzymatically synthesized pmPDA and GO-P200 composite, respectively. The solid lines were drawn using the Langmuir isotherm equation with optimum parameter values being estimated by the linear regression analysis of the experimental data.

Since our research objective was to synthesize and find the GO-pmPDA composites possessing high adsorption capacity for Pb^{2+}, we, therefore, selected GO, pmPDA, and GO-P200 to continue adsorption isotherm experiments to access and compare their adsorption properties and potential in more detail.

4. Adsorption Isotherms Studies

The adsorption isotherm experiments for GO, pmPDA and GO-P200 composite were carried out in distilled water containing varying concentrations of lead ions. The experimental data presented in Fig. 6 follow saturation isotherms at higher concentrations of Pb^{2+}.

The Langmuir adsorption isotherm typically describes the relation between q_e and C_e as

$$q_e=q_{max}K_LC_e/(1+K_LC_e) \quad (11)$$

where C_e (μmol/L) is the Pb^{2+} concentration in solution and q_e (μmol/g) is the specific Pb^{2+} adsorption capacity of adsorbents at equilibrium. The two parameters of Langmuir adsorption isotherm, K_L (L/μmol) and q_{max} (μmol/g), represent the Langmuir equilibrium constant and the maximum adsorption capacity of adsorbents, respectively. Table 3 lists the values of the estimated Langmuir isotherm parameters for GO, pmPDA, and GO-P200 composite from the linear regression analysis using the data in Fig. 6.

For the three adsorbents, K_L value was the smallest for pmPDA (2.332×10^{-3} L/μmol) and the largest for GO (8.024×10^{-3} L/μmol). GO-P200 has a K_L value of 4.219×10^{-3} L/μmol which is smaller than that of GO but almost twice that of pmPDA. The Langmuir constant, K_L, represents the interaction strength between the adsorbent and the adsorbate. The higher K_L value indicates that there exist stronger interactions between adsorbent and adsorbate while the lower K_L value implies weaker interactions [32]. It is well established that metal ions could be strongly bound to electron-rich functional groups like amino or hydroxyl groups by forming chelation or coordinate bonds. Both nitrogen and oxygen groups are known to have high affinity towards Pb^{2+} ions [33,34]. The amine group from a polymer such as NH_2 or NH contributes generally to selective adsorption of metal ions onto carbon-based materials, which are usually synergistic with the oxygen holding functional groups [35]. On the other hand, oxygen-based functional groups are so far the most important when it comes to influencing surface interaction, hydrophobicity, catalytic and electrical properties of carbon [35]. According to the larger K_L values for GO and GO-P200 composite than for pmPDA, we presume that the adsorption strength for Pb^{2+} of the oxygen-based functional groups in GO seems a little higher compared to the amine-based functional groups of pmPDA. GO is supposed to provide the oxygen-based functional groups of higher affinity for Pb^{2+} along with a higher surface area. Thus, even a small proportion of GO is known to enhance lead removal in several folds [36], which clarifies the significance of GO for the preparation of various composites.

Table 3. Langmuir isotherm parameters calculated by linear regression analysis

Adsorbents	q_{max}		K_L (L/μmol×10^3)	R^2 value
	μmol/g	mg/g		
pmPDA	564.7	117.0	2.332	0.9855
GO	984.3	203.9	8.024	0.9949
GO-P200	2164	448.5	4.219	0.9952

The maximum adsorption capacity (q_{max}) was 564.7, 984.3 and 2,164 (μmol/g) for pmPDA, GO and GO-P200, respectively. The q_{max} value for pmPDA was close to what we obtained previously [30]. Notably, GO-P200 expressed about four-times higher q_{max} value than pmPDA, indicating the significance of a unique composite combination of pmPDA and GO. In fact, the q_{max} value for GO-P200 was higher than most of the previously reported q_{max} values for other adsorbents [37-39]. One exceptional case was for the metal-organic framework in an applied magnetic field for which q_{max} value of 492.4 mg/g was reported [40]. However, note that GO-P200, which was synthesized by simple enzymatic catalysis of laccase in our study, reached the remarkable q_{max} value of 448.5 mg/g in a traditional uncomplicated manner without the help of an external force field.

CONCLUSIONS

We have promisingly demonstrated the application of polymeric composites as excellent adsorbent for the removal of Pb^{2+} ions from the aqueous waste effluents. Both pmPDA and GO-pmPDA composites were successfully synthesized by laccase-catalyzed enzymatic reaction in a benign condition. A unique combination proportion of GO and pmPDA was found out to be effective in adsorbing Pb^{2+} ions. The adsorption isotherms of GO, pmPDA and the combination of GO and pmPDA composite were performed and successfully expressed by the Langmuir adsorption isotherm model. The GO-P200 composite, for which a 1 : 1 mass ratio of GO and pmPDA monomer was used for the synthesis, exhibited a maximum adsorption capacity of ~2,164 μmol/g. The estimated content of composite was 56.1 wt% of pmPDA being estimated by

the thermogravimetric analysis (TGA). The synergistic effect of the high surface area of GO and functionality of both GO and pmPDA proved to improve the adsorption capacity of the composites for one of the most toxic heavy metal ions, Pb^{2+}, to a great extent. The composites showed unique and attractive characteristics needed for the remediation of Pb^{2+} ions, thus showing great promise in the field of wastewater treatment.

ACKNOWLEDGEMENTS

This research was supported by Basic Science Research Program through the National Research Foundation of Korea (NRF) funded by the Ministry of Education (2018R1D1A1B07049850).

REFERENCES

1. F. Fu and Q. Wang, *J. Environ. Manage.*, **92**, 407 (2011).
2. R. K. Sharma and M. Agrawal, *J. Environ. Biol.*, **26**, 301 (2005).
3. B. Alyuz and S. Veli, *J. Hazard. Mater.*, **167**, 482 (2009).
4. Y. S. Ho, *J. Hazard. Mater.*, **136**, 681 (2006).
5. C. A. Martínez-Huitle and E. Brillas, *Appl. Catal. B.*, **87**, 105 (2009).
6. A. K. Verma, R. R. Dash and P. Bhunia, *J. Environ. Manage.*, **93**, 154 (2012).
7. A. W. Zularisam, A. F. Ismail and R. Salim, *Desalination*, **194**, 211 (2006).
8. I. Hajdu, M. Bodnár, Z. Csikós, S. Wei, L. Daróczi, B. Kovács, Z. Győri, J. Tamás and J. Borbély, *J. Membr. Sci.*, **409**, 44 (2012).
9. S. Z. Mohammadi, M. A Karimi, D. Afzali and F. Mansouri, *Desalination*, **262**, 86 (2010).
10. M. R. Huang, Q. Y. Peng and X. G. Li, *Chem. Eur. J.*, **12**, 4341 (2006).
11. G. Tolian, S. A. Jafari and S. Zarei, *Water Pollut. Res. J. Can.*, **50**, 109 (2015).
12. B. Xiao and K. M. Thomas, *Langmuir*, **21**, 3892 (2005).
13. X. G. Li, M. R. Huang, W. Duan and Y. L. Yang, *Chem. Rev.*, **102**, 2925 (2002).
14. Z. Su, L. Zhang, L. Chai, H. Wang, W. Yu, T. Wang and J. Yang, *New J. Chem.*, **38**, 3984 (2014).
15. W. Yu, L. Zhang, H. Wang and L. Chai, *J. Hazard. Mater.*, **260**, 789 (2013).
16. M. J. Allen, V. C. Tung and R. B. Kaner, *Chem. Rev.*, **110**, 132 (2010).
17. D. R. Dreyer, S. Park, C. W. Bielawski and R. S. Ruoff, *Chem. Soc. Rev.*, **39**, 228 (2010).
18. H. Bai, K. Sheng, P. Zhang, C. Li and G. Shi, *J. Mater. Chem.*, **21**, 18653 (2011).
19. S. Chen, J. Zhu, X. Wu, Q. Han and X. Wang, *ACS Nano*, **4**, 2822 (2010).
20. J. Lee, J. Kim, S. Kim and D. H. Min, *Adv. Drug Deliv. Rev.*, **105**, 275 (2016).
21. X. D. Zhuang, Y. Chen, G. Liu, P. P. Li, C. X. Zhu, E. T. Kang, K. G. Noeh, B. Zhang, J. H. Zhu and Y. X. Li, *Adv. Mater.*, **22**, 1731 (2010).
22. K. Ryu, H. Xue and J. Park, *J. Chem. Technol. Biotechnol.*, **88**, 788 (2013).
23. W. Feng and P. Ji, *Biotechnol. Adv.*, **29**, 889 (2011).
24. S. Kobayashi and A. Makino, *Chem. Rev.*, **109**, 5288 (2009).
25. F. Zhang, B. Zheng, J. Zhang, X. Huang, H. Liu, S. Guo and J. Zhang, *J. Phys. Chem. C.*, **114**, 8469 (2010).
26. J. Park, N. Raseda, E. S. Oh and K. Ryu, *J. Appl. Polym. Sci.*, **133**, 43307 (2016).
27. Y. Xu, N. Raseda, I. K. Yoo and K. Ryu, *Can. J. Chem. Eng.*, **97**, 869 (2019).
28. N. Raseda, J. Park and K. Ryu, *Korean J. Chem. Eng.*, **33**, 3011 (2016).
29. V. H. Pham, T. V. Cuong, S. H. Hur, E. W. Shin, J. S. Kim, J. S. Chung and E. J. Kim, *Carbon*, **48**, 1945 (2010).
30. Y. Xu, I. K. Yoo, H. Lee and K. Ryu, *Chem. Pap.*, **73**, 1705 (2019).
31. O. Nabinejad, D. Sujan, M. E. Rahman and I. J. Davies, *J. Therm. Anal. Calorim.*, **122**, 227 (2015).
32. N. Deedar and I. Aslam, *J. Environ. Sci.*, **21**, 402 (2009).
33. S. Luo, X. Xu, G. Zhou, C. Liu, Y. Tang and Y. Liu, *J. Hazard. Mater.*, **274**, 145 (2014).
34. L. A. Bernal-Martínez, S. Hernández-López, C. Barrera-Díaz, F. Ureña-Núñez and B. Bilyeu, *Ind. Eng. Chem. Res.*, **47**, 1026 (2008).
35. X. Yang, Y. Wan, Y. Zheng, F. He, Z. Yu, J. Huang, H. Wang, Y. S. Ok, Y. Jiang and B. Gao, *Chem. Eng. J.*, **366**, 608 (2019).
36. R. P. Medina, E. T. Nadres, F. C. Ballesteros and D. F. Rodrigues, *Environ. Sci. Nano.*, **3**, 638 (2016).
37. S. Ai, Y. Huang, C. Huang, W. Yu and Z. Mao, *Environ. Sci. Pollut. Res.*, **28**, 2728 (2021).
38. S. Shahabuddin, C. Tashakori, M. A. Kamboh, Z. S. Korrani, R. Saidur, H. R. Nodeh and M. E. Bidhendi, *Environ. Sci.: Water Res. Technol.*, **4**, 549 (2018).
39. L. Fan, C. Luo, M. Sun, X. Li and H. Qiu, *Colloids Surf. B.*, **103**, 523 (2013).
40. R. Ricco, K. Konstas, M. J. Styles, J. J. Richardson, R. Babarao, K. Suzuki, P. Scopece and P. Falcaro, *J. Mater. Chem. A.*, **3**, 19822 (2015).